Molecular Vision 2018; 24:818-833 <http://www.molvis.org/molvis/v24/818>
Received 21 June 2018 | Accepted 28 December 2018 | Published 30 December 2018

Bulk changes in posterior scleral collagen microstructure in human high myopia

Petar P. Markov,[1] Ashkan Eliasy,[2] Jacek K. Pijanka,[1] Hla M. Htoon,[3] Neil G. Paterson,[4] Thomas Sorensen,[4] Ahmed Elsheikh,[2,5,7] Michael J.A. Girard,[3,6] Craig Boote[1,6]

[1]Structural Biophysics Research Group, School of Optometry and Vision Sciences, Cardiff University, Cardiff, UK; [2]Biomechanical Engineering Group, School of Engineering, University of Liverpool, Liverpool, UK; [3]Singapore Eye Research Institute (SERI), Singapore; [4]Diamond Light Source, Harwell Science and Innovation Campus, Harwell, UK; [5]NIHR Biomedical Research Centre for Ophthalmology, Moorfields Eye Hospital NHS Foundation Trust and UCL Institute of Ophthalmology, UK; [6]Ophthalmic Engineering & Innovation Laboratory (OEIL), Department of Biomedical Engineering, National University of Singapore, Singapore; [7]School of Biological Science and Biomedical Engineering, Beihang University, Beijing, China.

Purpose: We aimed to characterize any bulk changes in posterior scleral collagen fibril bundle architecture in human eyes with high myopia.

Methods: Wide-angle X-ray scattering (WAXS) was employed to map collagen orientation at 0.5 mm × 0.5 mm spatial intervals across the posterior sclera of seven non-myopic human eyes and three eyes with high myopia (>6D of refractive error). At each sampled point, WAXS provided thickness-averaged measures of the angular distribution of preferentially aligned collagen fibrils within the tissue plane and the anisotropic proportion (the ratio of preferentially aligned to total collagen scatter).

Results: Non-myopic specimens featured well-conserved microstructural features, including strong uniaxial collagen alignment along the extraocular muscle insertion sites of the mid-posterior sclera and a highly anisotropic annulus of collagen circumscribing the nerve head in the peripapillary sclera. All three myopic specimens exhibited notable alterations in the peripapillary sclera, including a partial loss of circumferential collagen alignment and a redistribution of the normally observed regional pattern of collagen anisotropic proportion. Linear mixed-model analysis indicated that the mean fiber angle deviation from the circumferential orientation in the peripapillary sclera of highly myopic eyes (23.9° ± 18.2) was statistically significantly higher than that of controls (17.9° ± 12.0; $p<0.05$).

Conclusions: Bulk alterations in the normal posterior scleral collagen microstructure occur in human eyes with high myopia. These changes could reflect remodeling of the posterior sclera during axial lengthening and/or a mechanical adaption to tissue stresses induced by fluid pressure or eye movements that may be exacerbated in enlarged eyes.

Myopia is the most common visual disorder, affecting an estimated one quarter of the world's population, with the number expected to reach one half by 2050 [1]. Myopia is a type of refractive error defined by the inability to see at greater distances and is caused, in major part, by an abnormal axial lengthening of the globe—placing the eye's focal plane in front of the retina. Individuals with myopia exceeding 6D are classified as having high myopia [2-4] and are at increased risk of developing further complications that can lead to temporary or permanent loss of vision, including glaucoma, cataract, macular degeneration, and retinal detachment [5]. As the prevalence of myopia continues to rise, gaining control of the escalating myopia problem is becoming a growing global concern [6].

Correspondence to: Craig Boote, Cardiff University, School of Optometry and Vision Sciences, Maindy Road, Cardiff CF24 4HQ UK; Phone: +44 (0)2920 870586; FAX: +44 (0)292087 4859; email: bootec@cardiff.ac.uk

Myopic lengthening of the eye involves remodeling and biomechanical changes in the eye's main load-bearing tissue—the sclera, the white fibrous tissue that comprises about 85% of the ocular tunic [7]. The sclera consists predominantly of densely woven fibrils of the complex protein collagen that impart the tissue with mechanical rigidity and which, in turn, helps maintain the eye's structural integrity and shape [8]. In the human sclera, about 90% of the dry weight is due to collagen. After being secreted into the extracellular space, collagen molecules assemble into fibrils, which have a wide range of diameters from 25 to 230 nm [9] and span many hundreds of microns in length in mature tissues [10]. The collagen fibril bundles in the sclera are more complex and generally more disorganized than in the neighboring cornea and show a high degree of regional variability in their bulk orientation between different areas of the tunic [11-13]. The collagen architecture of the posterior sclera plays a major role in governing tissue deformation in response to changes in intraocular pressure (IOP) and cerebrospinal fluid pressure (CSFP), and scleral stresses are

readily transmitted to the more compliant tissues of the optic nerve head (ONH) [12,14]. The ONH may be considered a "weak spot" in the scleral tunic, where the sieve-like lamina cribrosa (LC) supports the existing nerve axons, and where deformation forces are accumulated, making it an area of particular mechanical interest [15,16].

Several alterations to the scleral structure and neighboring tissues have been noted to occur with high myopia. With axial elongation of the eye globe, the sclera, the LC, and the choroid have been noted to become thinner [17-19]. Sclera growth and remodeling in the myopic eye is considered to be a dual process [20,21]. The amount of collagen decreases by downregulation in the synthesis of type I collagen and concomitant stimulation of collagen degradation [22,23]. The end result is a decline in existing collagen bundles and prevention of the formation of new ones. A decrease in the collagen fibril diameter, particularly near the posterior pole, has also been noted [24]. Studies in mammalian models further confirm that the changes during myopia development are the result of active tissue remodeling rather than just passive stretching of the sclera, contributing to a compromise in the mechanical stability and integrity of the tissue [25,26]. However, although there is substantial evidence that collagen remodeling underlies the axial elongation of the myopic sclera [20-26], it is not known to what extent this process manifests in terms of bulk changes in the orientation of collagen in the tunic, a key determinant of its direction-dependent biomechanical properties. Previously, we applied wide-angle X-ray scattering (WAXS) to map the collagen fibrillar architecture in normal and glaucomatous posterior scleral shells [12,13]. The goal of the present study was to apply these methods to evaluate any bulk changes to collagen orientation in the posterior sclera of highly myopic human eyes.

METHODS

Tissue details and sample preparation: All experimental procedures were conducted in accordance with the WMA Declaration of Helsinki on Ethical Principles for Medical Research Involving Human Subjects. The study was approved by the NHS-HRA Wales Research Ethics Committee. Nine human ocular globes (seven non-myopic and two highly myopic) were obtained from the Fondazione Banca degli Occhi del Veneto, Italy. In addition, one additional highly myopic eye was obtained from the Department of Ophthalmology, University of Hong Kong. All specimens were acquired within a 13–18 h window after death. Following removal of the ocular contents, the intact scleral shells were stored in 4% paraformaldehyde at 277 K. The myopic or normal status (>6D for highly myopic) of the eyes was designated via examination by an ophthalmologist, and none had a history of previous surgery involving the posterior sclera. Furthermore, using the polar vector plot maps of collagen orientation from the WAXS experiments, we measured the distance between landmarks of the optic nerve canal edge and the insertions of the inferior oblique muscle, as a measure of the degree of scleral lengthening (Figure 1, Table 1). Scleral specimens were prepared based on previously established protocols [12,13]. The surrounding fat, muscle, and episcleral tissues were carefully removed before the optic nerve was excised with a razor blade flush to the sclera [13]. The cleaned globes were dissected around the equator and the internal lens, retina, and choroid and subsequently removed. To prevent the formation of creases when the posterior cups were flat mounted, relaxing meridional incisions were made in the posterior sclera from the equator to just outside the peripapillary region, defined as the 1.5 mm-wide annular scleral region immediately adjacent to the optic nerve canal opening. The specimens were then returned to 4% paraformaldehyde until the time of the X-ray experiments. As shown in our previous work, this mild fixation does not affect WAXS orientation measurements [27]. Details of the eyes used in this study are provided in Table 1. The mean donor age for the control group of seven non-myopic eyes was 66.3 ± 7.1 years, while the mean donor age of the three highly myopic specimens was 66.7 ± 8.3 years.

X-ray scattering data collection: Previously, our group developed a method for quantifying the bulk collagen fiber orientation of the sclera using WAXS [12,13]. When incident monochromatic X-rays pass through the sclera, a portion of them are scattered at different angles, and their direction will reflect the sclera's intrinsic microstructure. A well-resolved single diffraction peak is formed perpendicular to the fibril axis, referred to as the equatorial direction. This scatter pattern arises from the regular 1.6 nm lateral packing of the collagen molecules that make up the fibrils [28]. The angular intensity distribution can be analyzed to quantify the number of fibrils in each direction within the tissue plane. A key advantage of this approach is that the scleral tissue is not required to be sectioned, embedded, or stained for the experiments, thus preventing artificial disruptions in the microstructure. Moreover, irrespective of the varying diameter and packing of scleral collagen fibrils across the eye tunic, the diameter and the packing of the constituent collagen molecules from which the WAXS signal originates are highly uniform, which give rise to a sharp well-resolved signal that is relatively impervious to variations in tissue hydration [12]. The technique provides quantification of the collagen orientations as an average of the tissue thickness [29].

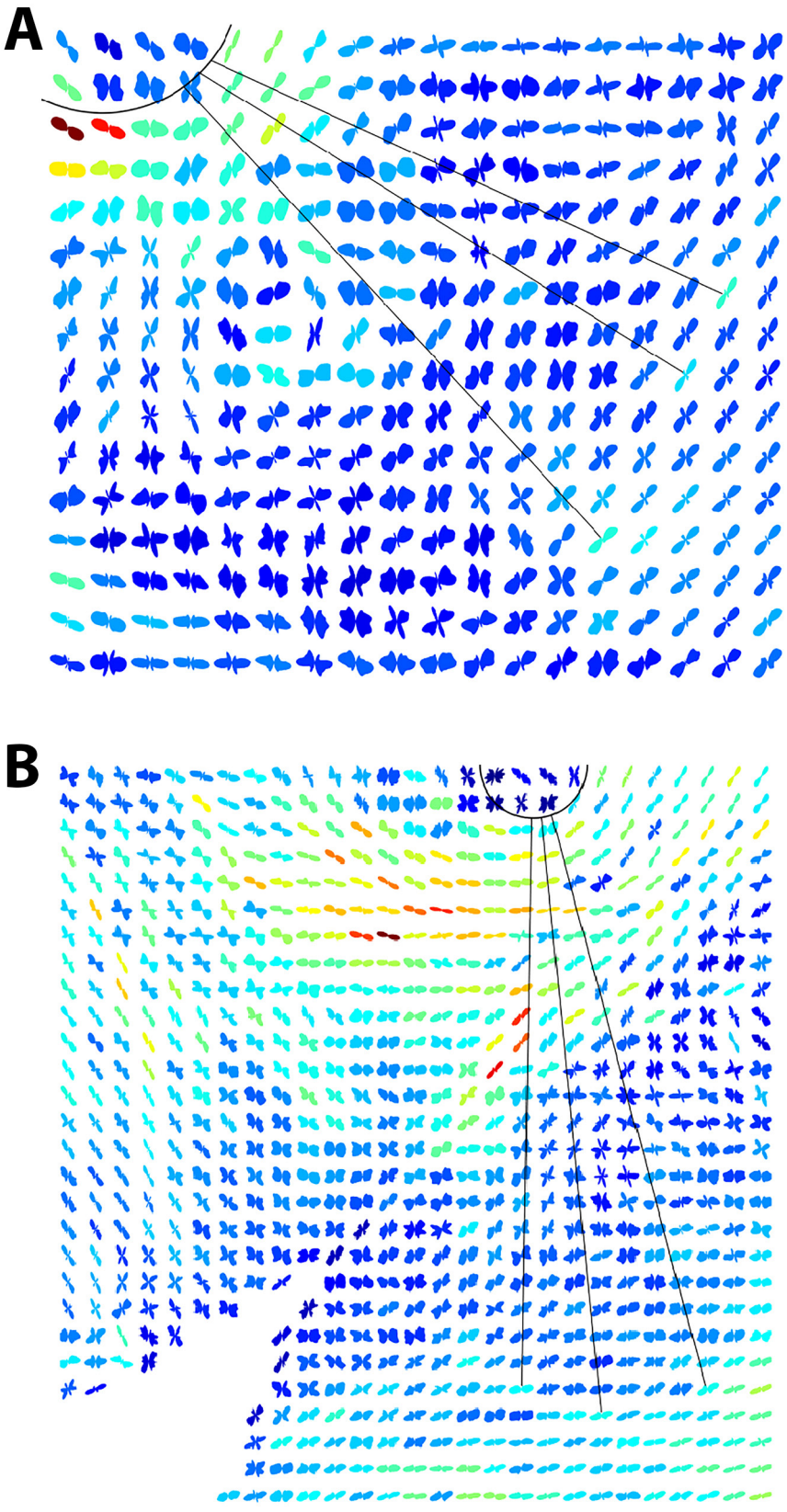

Figure 1. Calculating the distance between the edge of the optic nerve canal and the tendon insertions of the inferior oblique muscle. Wide-angle X-ray scattering (WAXS) polar vector plots (plot interval: 0.5 mm) reveal circumferential collagen annulus around the canal and the oblique uniaxial alignment of the muscle insertion region. The canal edge is denoted by a curved line. Three individual measurements (line lengths) were performed and a mean taken as the representative value. **A**: Non-myopic posterior sclera N6. **B**: Highly myopic specimen HM2. Note the marked increase in line length for the myopic specimen, indicative of the axial lengthening of the globe.

Table 1. Details of the eye specimens used in the current study.

Specimen	N1	N2	N3	N4	N5	N6	N7	HM1	HM2	HM3
Age	75	75	64	65	53	63	69	60	64	76
Left/Right	Left	Right	Left	Right	Right	Right	Left	Left	Right	Left
Myopic Status	Normal	Normal	Normal	Normal	Normal	Normal	Normal	Highly Myopic	Highly Myopic	Highly Myopic
ONH-IO distance [mm]	9.49	9.41	9.29	9.14	9.78	8.66	9.59	N.A.	12.57	10.80

Optic nerve head (ONH) canal edge to inferior oblique (IO) muscle insertion distance is included as a measure of relative axial globe elongation for all specimens, apart from HM1 which was not measurable (as denoted N.A.). Note the consistent ONH-IO distance for normal (non-myopic) specimens, which was markedly increased for highly myopic specimens HM2 and HM3.

WAXS experiments were conducted at the Diamond Light Source (Harwell, UK), the UK's national synchrotron facility. The specimens were measured using macromolecular crystallography beamlines I02 and I03, which have identical capabilities. The beamlines were operated in a custom-modified fiber-diffraction set-up to record WAXS patterns across each scleral sample at 0.5 mm (horizontal) × 0.5 mm (vertical) intervals using an integrated x-y motor stage (Figure 2) [12,30]. The whole of each posterior scleral cup was scanned for all specimens, apart from highly myopic specimen HM3, where only a 16 mm × 16 mm square region centered on the ONH was available for the study. To prevent tissue dehydration during data collection, the specimens were wrapped in polyvinylidene chloride film and mounted inside Perspex (Lucite Group Ltd, Southampton, UK) chambers with Mylar (DuPont-Teijin, Middlesbrough, UK) windows. The incident X-ray beam was directed perpendicular to the specimen surface, with an exposure time of 1 s or 0.5 s and recorded electronically on a Pilatus-6MF silicon pixel detector (Dectris Ltd, Baden, Switzerland) placed 350 mm behind the specimen. The wavelength of the focused beam was 0.09795 nm with a 150 µm × 80 µm cross-section.

X-ray scattering data processing: By analyzing the angular distribution of intensity around the 1.6 nm WAXS reflection (Figure 3A), a quantitative measure of the relative number of collagen fibrils oriented at a given angle within the scleral plane can be acquired. We obtained the following from all

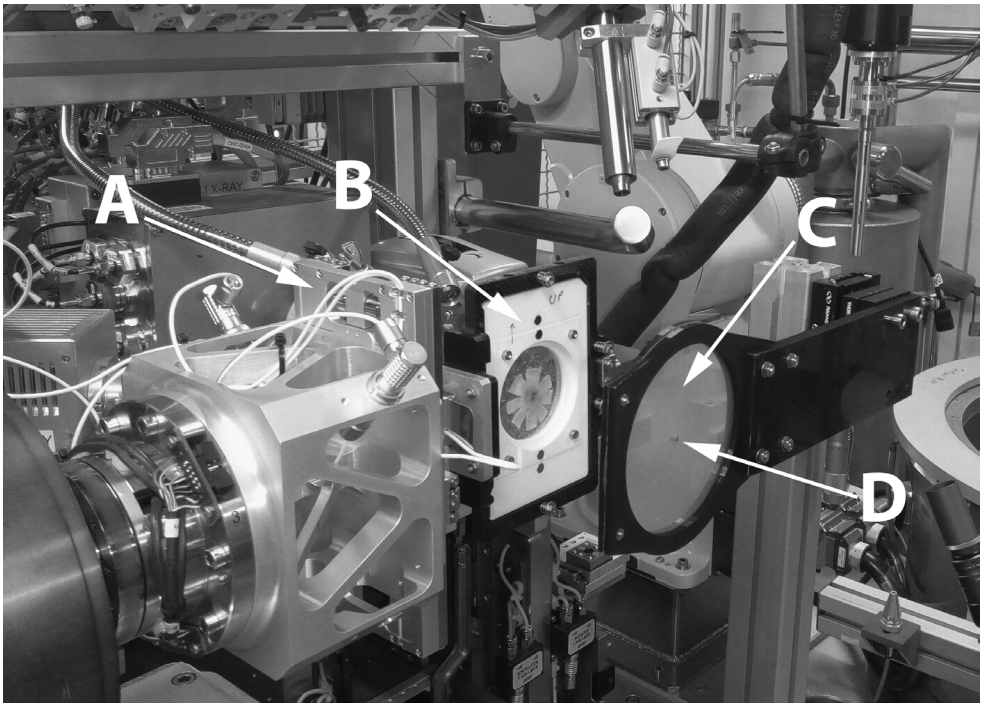

Figure 2. Beamline I03 at the Diamond Light Source operating in a custom fiber-diffraction set-up. The goniometer (**A**) provides directional translation of the sample holder (**B**) between X-ray exposures. A flat-mounted posterior sclera is shown mounted between Mylar sheets. After the specimen is positioned, an additional Mylar sheet (**C**) in which a lead beam stop (**D**) is attached prevents undiffracted X-rays from reaching and damaging the detector positioned out of shot.

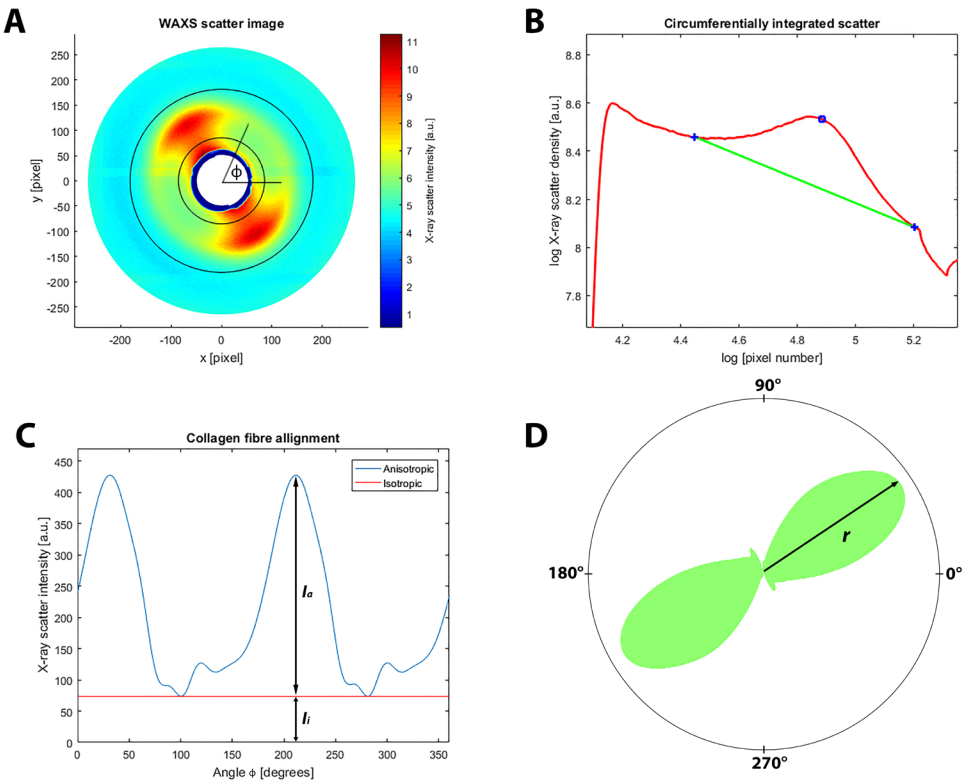

Figure 3. X-ray scattering data analysis. **A**: Wide-angle X-ray scattering (WAXS) pattern from peripapillary human sclera N4. The area bounded by the two concentric circles corresponds to the collagen scatter. The X-ray scatter intensity spread as a function of the azimuth angle ϕ around the collagen peak can be analyzed, which provides the distribution of the fibril orientations. The presented two-lobed WAXS pattern is indicative of the uniaxial fiber alignment at that point in the tissue. **B**: Power-law background function (green line) fitted to a radial intensity profile (red line) through the pattern shown in (**A**). The blue open circle marks the peak in collagen intensity, while the blue crosses show the fitting points of the background function. For each WAXS pattern, a background function was independently fitted along the 720 equally spaced radial directions, which allows extraction of the collagen signal in two dimensions. **C**: Angular X-ray scatter intensity profile for the pattern presented in (**A**). The collagen scatter intensity may be represented as two components: scatter from the isotropically aligned collagen fibrils (*Ii*) and anisotropic scatter (*Ia*) arising from preferentially aligned collagen. **D**: Corresponding polar vector plot of the collagen alignment. The anisotropic collagen scatter is displayed in polar coordinates, where the length of vector **r** is proportional to the relative number of collagen fibrils oriented along the preferred direction.

specimens at each sampled point in the tissue: 1) the relative number of preferentially aligned fibrils at a given angle over and above the underlying isotropic population, referred to as the collagen orientation distribution, with the magnitude of the principal direction representing the collagen anisotropy, and 2) the scatter due to preferentially aligned collagen divided by that from the total fibrillar collagen content, referred to as the anisotropic proportion.

The quantification of the scleral fiber collagen orientation from WAXS patterns is described in detail elsewhere [12,28]. In brief, the scatter profiles were analyzed using a bespoke MATLAB software script (MATLAB; MathWorks, Natick, MA) that adapted a previously used approach [12,31]. A total of 720 radial profiles (one every 0.5°) were extracted from each WAXS pattern, and a unique power-law background function was fitted and subtracted from each (Figure 3B) [12,13,30]. The isolated scatter profiles along each direction were normalized against the X-ray beam current fluctuations and exposure time, radially integrated, and the values extracted to angular bins. The resulting angular intensity profiles were divided into two components: isotropic and anisotropic scatter (Figure 3C). The latter was plotted in polar vector coordinates. To take into account that equatorial scatter occurs at right angles to the collagen axis, a 90° shift in the total collagen scatter distribution was performed. For each sampled point in the scleral tissue, the collagen orientation distribution could be represented with a polar vector plot (Figure 3D). Individual plots were then assimilated into montages, and the anisotropy assigned color codes in MATLAB, representative of the highest degree of alignment (maximum vector length per plot). Contour maps of collagen anisotropic proportion were generated in MATLAB, by calculating the ratio of aligned against total integral collagen scatter (Equation 1):

$$Anisotropic\ proportion = \frac{\int_{o}^{2\pi} I_a d\phi}{\int_{o}^{2\pi} (I_a + I_i) d\phi}$$

where I_a is the preferentially aligned collagen scatter (i.e., above the isotropic threshold I_i) at angle ϕ (Figure 3C), and ϕ is the azimuthal fiber angle in the tissue plane (Figure 3A). To compare bulk collagen structural changes between myopic and non-myopic individuals, we selected a fixed region of 64 sampling points within a 1.5 mm radius of the optic nerve canal edge, representative of the peripapillary scleral region [12]. Sampling points outside this region were considered part of the mid-posterior sclera. The peripapillary sclera was further divided into four quadrants based on their position: superior-nasal (SN), superior-temporal (ST), inferior-temporal (IT), and inferior-nasal (IN). For all of the sub-regions, an average for the collagen anisotropy was calculated. To quantify any distortion in the alignment direction of the preferentially aligned collagen bundles in the peripapillary sclera, we compared the angular displacement of the main direction revealed by the polar vector plots (for individual myopic specimens and the averaged control) to an idealized angle distribution representative of the circumferential collagen fiber structure circumscribing the optic nerve that characterizes the normal human sclera [12,13,32]. The idealized distribution model (Appendix 1) was created in MATLAB and consists of one partial inner ring and three full outer rings of polar vector plots (total angular range: 0° to 180°). The distribution width of the idealized plot (dispersion around the main orientation) was computed from the average of the experimentally determined peripapillary scleral plots from the control specimens. Within each quadrant of the distribution, there are n + 2 polar plots per ring (0°/180° and 90° are omitted from the partial inner ring) and a 90 / (n + 1) angular step, where n is the radial position of the ring with respect to the scleral canal edge (1 being the closest). This resulted in a total of 16 plots per quadrant, matching the spatial sampling of the peripapillary sclera in the WAXS experiments, arranged in as close to the circumferential orientation as possible.

Statistical analysis: For statistical assessment of the differences in the collagen anisotropic proportion and the main fiber alignment direction between the highly myopic and control eyes, we leveraged the 64 unique spatial measurements recorded per eye from the peripapillary sclera and performed a linear mixed-model analysis for repeated measures (considered a nested variable) using SPSS software ver. 24.0 (IBM Corp., Armonk, NY). Linear mixed-model analysis allows for marginal estimations through the increase in observations in the cluster variable, maximizing the statistical power of the analysis. For statistical analysis, data from control specimens N1 and N2 (a pair from the same donor) were first averaged point for point. For the mixed models, a compound symmetry variance and covariance structure was selected according to the smaller the better information basis, based on Hurvich and Tsai's criterion for small sample sizes (the other structures compared were first-order autoregressive and diagonal). A probability threshold of $p<0.05$ was considered statistically significant for the mean differences in the anisotropic proportion and the fiber deviation angle (from the circumferential orientation) between the control (n=6) and highly myopic (n=3) groups.

RESULTS

In Figure 4, a polar plot map of collagen orientation is presented. The map is overlaid on top of a photograph of the scanned posterior sclera of a non-myopic right human eye (specimen N4). In accordance with previous WAXS studies, reproducible structural features characteristic of the non-myopic sclera were found [12,13]. These features included the tendon insertions of the inferior oblique muscle in the mid-posterior region, which were found to be consistent in position from the landmark of the optic nerve canal (Table 1). Around the optic nerve, the collagen bundles were preferentially aligned in a circumferential direction, and this feature exhibited noticeably higher collagen anisotropy. Another consistent feature was two linear fiber bands that radiated tangentially from the peripapillary ring of the aligned collagen outward into the mid-posterior scleral region [33]. All of these features were found to be present in the other six non-myopic specimens from the control group (see Supplemental Material).

In Figure 5, a comparison between a typical non-myopic scleral polar vector map and the three highly myopic specimens is presented and reveals several marked differences in the bulk collagen orientation. In the non-myopic specimens, there is consistently a disruption in the circumferential collagen orientation in the SN quadrant of the peripapillary sclera, as found in previous studies [12,13] (Figure 5B). However, for myopic specimen HM1 two such regions of disruption were observed instead, in the ST and IN regions (Figure 5D). HM2 exhibited more widespread differences: the ONH appears wider, and the surrounding annulus of collagen, which had a noticeably larger interruption in its circumferential structure in the SN quadrant, was spread over a larger radial distance, extending well into the mid-posterior sclera (Figure 5F). HM3 also featured a larger SN interruption to the normal circumferential structure (Figure 5G) and a noticeable splitting of the fiber alignment into two sub-populations over the majority of the peripapillary sclera. In particular, peripapillary fibers in HM2 and HM3 showed a move away from circumferential alignment toward the radial direction (Figure 5F,G).

For each sampled point of the posterior sclera, a value for the ratio of the aligned to total collagen (the anisotropic proportion) was also extracted and plotted (Figure 6). The anisotropic proportion values of the peripapillary sclera for the seven non-myopic posterior scleral specimens were combined into an averaged control. This was justified based on the highly conserved collagen structure of the posterior sclera in non-diseased eyes, as shown in this report and previously [12]. Regional quantification of this data is shown in Figure 7. For all seven non-myopic specimens, the minimum collagen anisotropic proportion was consistently observed in the SN quadrant, and the maximum value was observed in the IN quadrant (Appendix 2 and Figure 7). This pattern was not exhibited in the highly myopic specimens HM1 and HM2, where the minimum value was in the ST and IT and the maximum in the IT and ST quadrants, while HM3 displayed a maximum anisotropic proportion in the IT quadrant (Figure 7). The atypical results for the myopic sclera are highlighted in Figure 7, where the myopic specimen values (apart from the SN quadrant of HM3) are clearly identifiable as outliers to the box-plot data. The anisotropic proportion for the peripapillary sclera in specimen HM2 generally demonstrated higher values than the controls, HM1 and HM3 (Figure 6B,D,F,G). This appeared initially at odds with the vector plot maps, which indicated overall lower collagen anisotropy for HM2 around the nerve head (Figure 5B,D,F,G). However, the two observations may be reconciled if we consider that the collagen anisotropy scales directly with tissue thickness (and thus, the total collagen scatter), whereas the anisotropic proportion scales inversely with thickness. Therefore, it is likely that excessive tissue thinning around the posterior pole in myopic specimen HM2 would have manifested in a lower total collagen scatter, and thus, a higher anisotropic proportion, while the absolute number of fibrils along the preferred direction (defining the collagen anisotropy) was low. This would also be consistent with HM2 showing the largest indications of scleral lengthening, as determined by the inferior oblique muscle to the posterior pole distance (Table 1). Statistical comparison of the difference in the mean collagen anisotropic proportion in the whole peripapillary sclera between the control (n=6) and highly myopic (n=3) groups using linear mixed-model analysis fell below the $p<0.05$ statistical significance threshold (Figure 8A). This is likely because of the canceling effect of some tissue quadrants showing increases, and some decreases, with myopia. The

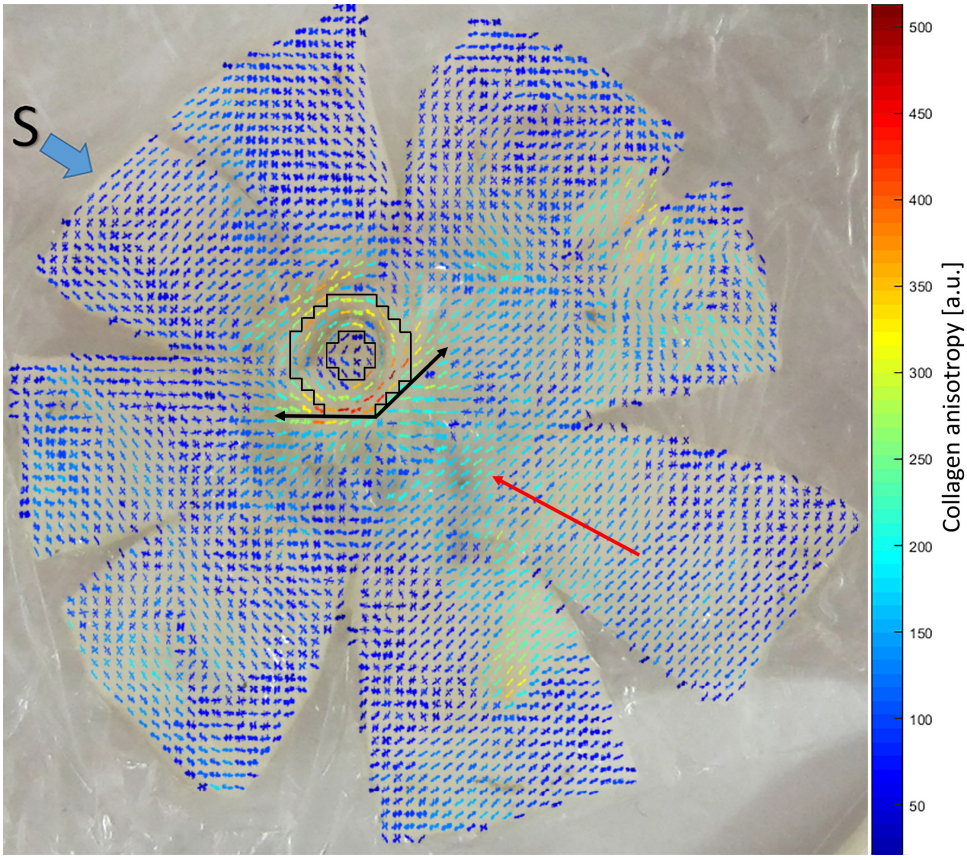

Figure 4. WAXS polar vector map showing preferential collagen orientation across non-myopic flat-mounted posterior sclera N4, overlaid over a photograph of the tissue before scanning. The superior direction of the specimen is indicated with a blue arrow. Polar vectors are color coded according to the bar, with warmer colors indicating higher degrees of collagen anisotropy. Note the highly aligned collagen annulus circumscribing the nerve head (the black line bounded region), two tangential fiber bands (black arrows), and the uniaxial alignment of the ocular muscle insertion regions, with the inferior oblique highlighted (red arrow).

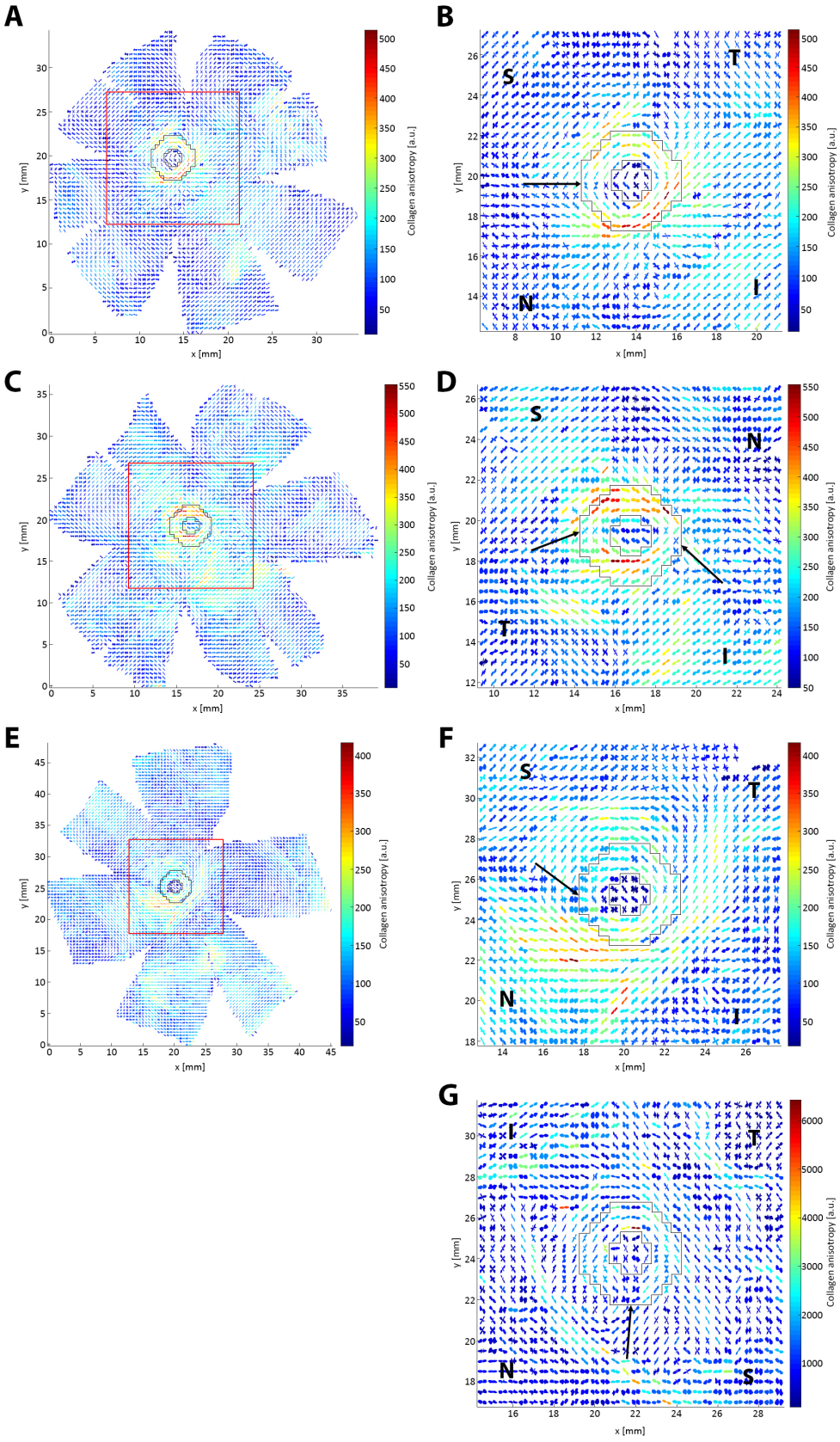

Figure 5. WAXS polar plot vector maps comparing one non-myopic (**A**–**B**) and two highly myopic (**C**–**F**) posterior scleras. **A**: Full map of non-myopic specimen N4. **B**: 30 × 30 vector plot zoom of N4. **C**: Full map of highly myopic specimen HM1. **D**: 30 × 30 vector plot zoom of HM1. **E**: Full map of highly myopic specimen HM2. **F**: 30 × 30 vector plot zoom of HM2. **G**: Map of myopic specimen HM3. The zoomed regions are denoted by a red square on the full maps. The peripapillary scleral region is shown bounded by black lines, in which largely circumferential collagen alignment is observed. Arrows: interruption of the circumferential collagen orientation (normally limited to the SN quadrant in non-myopic eyes) is more extensive in highly myopic specimens. **S**, **N**, **I**, and **T** denote the superior, nasal, inferior, and temporal directions, respectively.

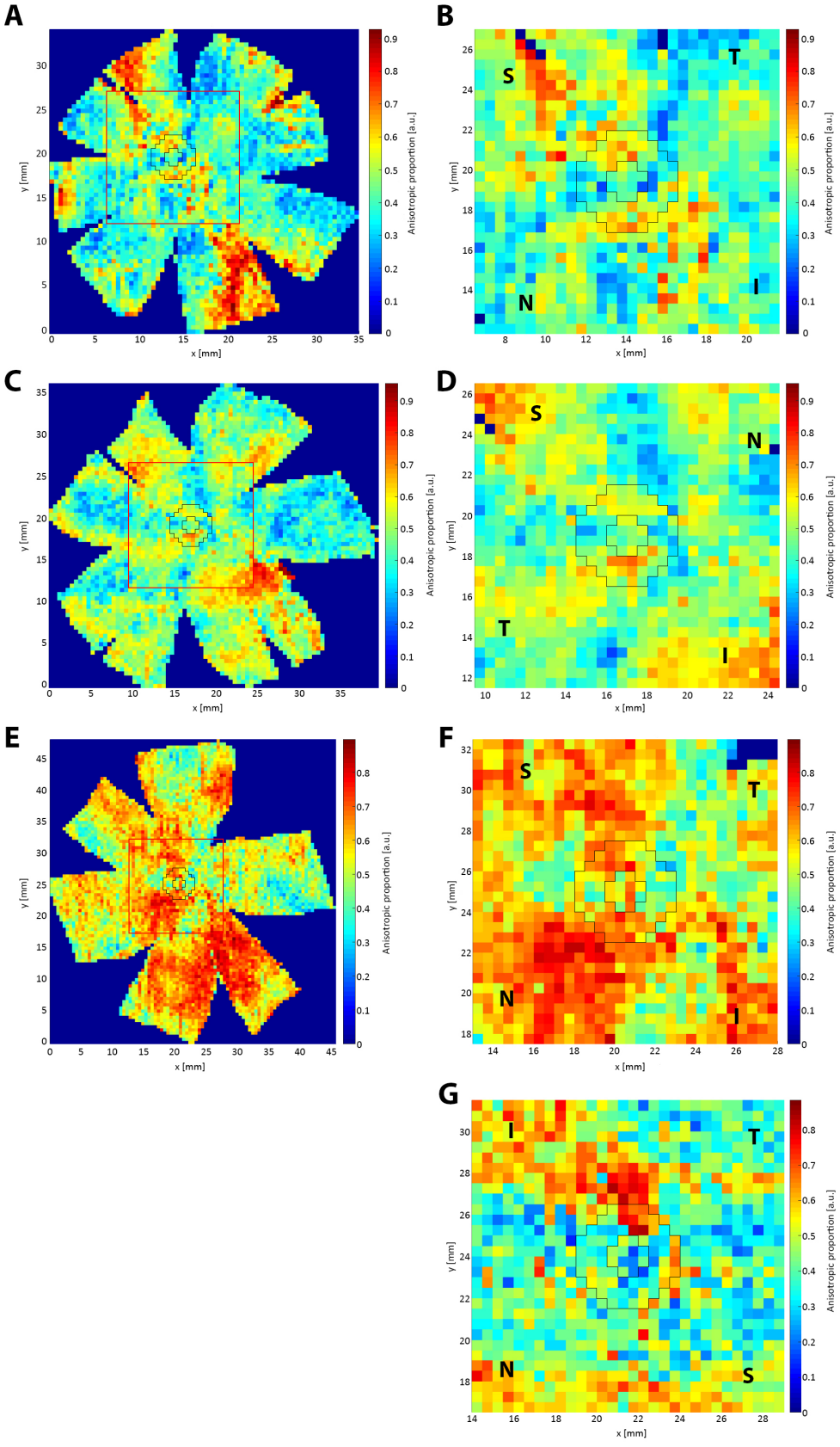

Figure 6. WAXS contour maps of collagen anisotropic proportion for one non-myopic (**A**–**B**) and two highly myopic (**C**–**F**) posterior scleras. **A**: Full map of non-myopic specimen N4. **B**: 30 × 30 point zoom of N4. **C**: Full map of highly myopic specimen HM1. **D**: 30 × 30 point zoom of HM1. **E**: Full map of highly myopic specimen HM2. **F**: 30 × 30 point zoom of HM2. **G**: Map of myopic specimen HM3. The zoom regions are denoted by a red square on the full maps. Peripapillary scleral region is shown bounded by black lines. **S**, **N**, **I**, and **T** denote the superior, nasal, inferior, and temporal directions, respectively.

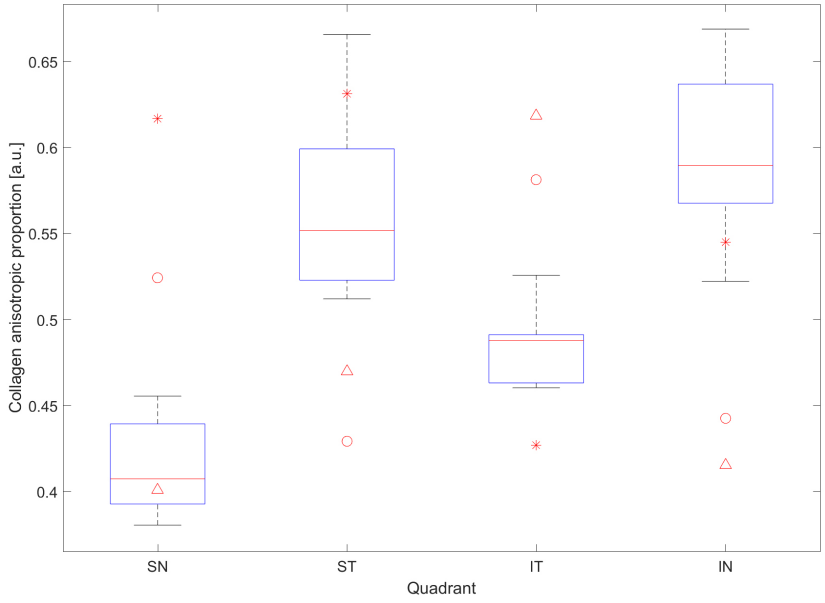

Figure 7. Box plots of the mean collagen anisotropic proportion in the peripapillary sclera by quadrant for the non-myopic control group (SN: superior-nasal, ST: superior-temporal, IT: inferior-temporal, IN: inferior-nasal). Specimen-specific corresponding values for highly myopic specimens HM1, HM2, and HM3 are shown for comparison and denoted by circles, asterisks, and triangles, respectively. Note that the majority of the myopic data lie outside the non-myopic range.

sample numbers were insufficient to conduct a quadrant-wise statistical comparison.

To further quantify the structural differences between the non-myopic control group and the two highly myopic eyes, we compared the angular displacement of the collagen vector plots from an idealized circumferential distribution (Appendix 1). The right eye was chosen as the default, and for the left eyes, a mirror image of the polar vector maps was taken. Figure 9 shows maps of the angle difference between the idealized circumferential distribution and (A) averaged control, (B) myopic specimen HM1, (C) myopic specimen HM2, and (D) myopic specimen HM3. The results indicate how closely the non-myopic structure follows the idealized circumferential orientation around the ONH (Figure 9A). HM1 followed the pattern to a lesser degree and diverged markedly from the idealized distribution in the ST quadrant with a maximum deviation of 74° (Figure 9B). For HM2, the differences were most pronounced on the outer parts of the peripapillary region in the SN quadrant, with a maximum deviation of 83° (Figure 9C). For HM3, the SN disturbances were again the most pronounced, with a maximum deviation of 79° (Figure 9D). These differences are further highlighted in the box-plot data in Figure 10, where the majority of the HM data are again visible as outliers to the control data. The mean fiber deviation (from the circumferential orientation) in the whole peripapillary sclera was statistically different between the control (17.9° ± 12.0, n=6) and highly myopic (23.9° ± 18.2, n=3) groups ($p<0.05$) using linear mixed-model analysis (Figure 8B).

DISCUSSION

This paper presents the first application of WAXS mapping to determine bulk collagen orientation changes in human eyes with high myopia. The results verify that in non-myopic human posterior sclera the collagen orientation distribution is highly conserved between individuals, while in specimens with high myopia a marked loss of the normal microstructural organization was observed. Previous research has

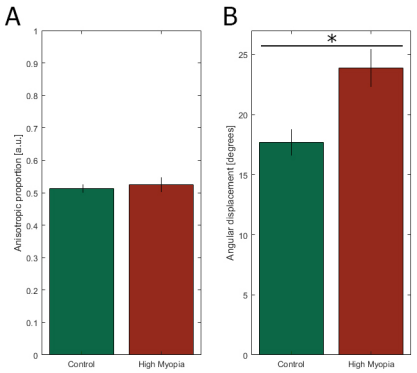

Figure 8. Group-wise statistical comparison of the mean (**A**) collagen anisotropic proportion and (**B**) the fiber angle deviation from circumferential in the whole peripapillary sclera using linear mixed-model analysis. The asterisk denotes statistical significance at the $p<0.05$ level.

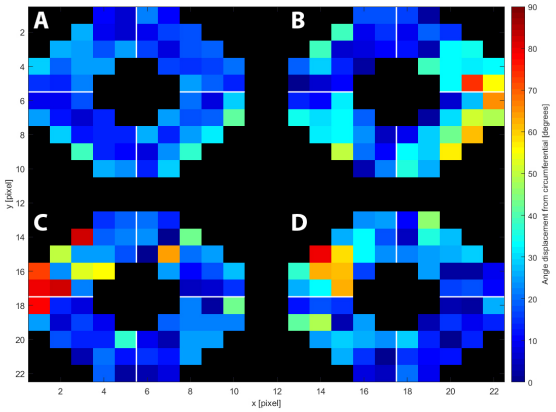

Figure 9. Variation from idealized circumferential angle distribution (with respect to the nerve canal edge) of the polar vector plots from the peripapillary sclera. The averaged control (**A**) is shown alongside the three highly myopic specimens HM1 (**B**), HM2 (**C**), and HM3 (**D**) following the orientation of a right eye viewed from the back: Top, superior; Left, nasal; Bottom, inferior; Right, temporal. Marked deviations from circumferential alignment show up as hot-spots in the myopic maps.

provided evidence for remodeling of the scleral extracellular matrix with myopia progression [21,34]. However, until now how bulk scleral collagen fibril orientation is affected in myopia has remained unknown. The present results provide evidence that highly myopic posterior sclera do not follow the normal fibrillar organization, with all three myopic specimens exhibiting notable changes in the peripapillary sclera. Specifically, the high myopia group showed a statistically significant increase in fiber angle deviation away from the normal circumferential arrangement with more radially oriented fibers present in the peripapillary sclera overall. Notable regional variations among the three myopic specimens likely reflect different stages of myopic lengthening, rather than natural variations between individual patients, as we established in this study and previously [12] that the collagen microstructure of the peripapillary sclera is well conserved between individuals not affected by posterior scleral disease. Unfortunately, the limited number of highly myopic specimens available to the study precluded us from being able to statistically compare individual high myopia specimens either with each other or to the control group, or to carry out a quadrant-wise analysis within the peripapillary sclera.

The existence of a distinct ring of peripapillary collagen fibers around the optic nerve was reported for the first time less than a decade ago and since then has been documented to exist in humans, as well as several animal species [27,31,35-38]. The circumferentially oriented fibril bundles provide mechanical stability to the ONH as they limit the IOP-related expansion of the scleral canal and reduce the in-plane tensile strains within the LC [14,16,29,39,40]. Thus, changes to the peripapillary collagen architecture in myopia may be linked to an increased susceptibility to ONH damage in glaucoma [12,41,42]. All highly myopic specimens in this study

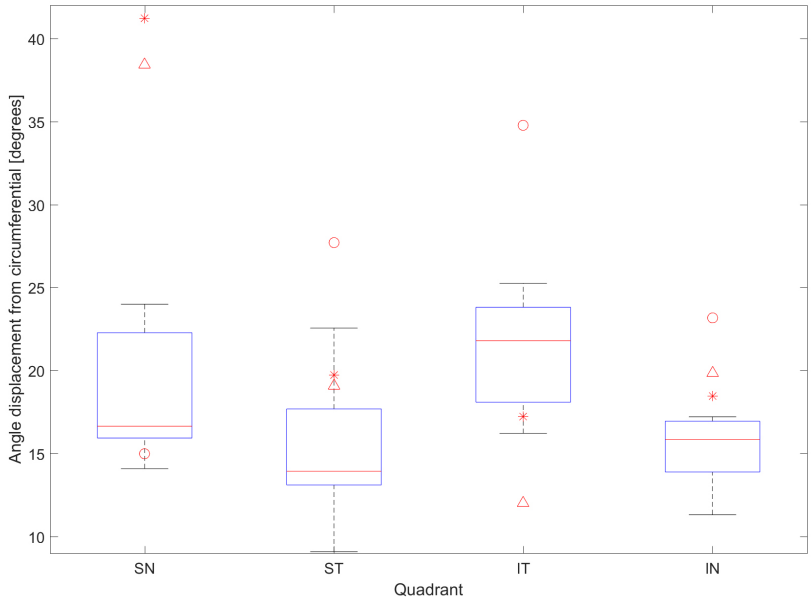

Figure 10. Box plots of mean collagen fiber deviation from circumferential orientation in the peripapillary sclera by quadrant for the non-myopic control group (SN: superior-nasal, ST: superior-temporal, IT: inferior-temporal, IN: inferior-nasal). Specimen-specific corresponding values for highly myopic specimens HM1, HM2, and HM3 are shown for comparison and denoted by circles, asterisks, and triangles, respectively. Note that the majority of the myopic data lie outside the non-myopic range.

displayed noticeable disruption in the preferential orientation of the collagen fibrils around the ONH. It is possible that remodeling of the extracellular matrix has occurred as a result of myopia, and that given the mechanical role of the peripapillary sclera, this may, in turn, affect the mechanical environment of the ONH and its physical response to IOP and CSFP fluctuations [14,41,43,44].

Although the structural changes reported here could be a consequence of scleral remodeling during axial lengthening, a further conceivable possibility is that they may represent a mechanical adaptation to increased tissue stresses in an enlarged eye. In respect of this, a change in the collagen fiber orientation in myopic eyes could potentially be due to loads other than IOP and CSFP. During horizontal eye movements, the optic nerve can exert a traction force on the eye globe to shear and deform the ONH tissues [45,46]. In high myopia, the optic nerve traction force could be considerably increased because of the elongated eyeball, thus, yielding a higher amount of optic nerve straightening for the ONH to travel the same distance as that in a healthy eye. In highly myopic eyes with staphylomas, it has also been shown that the optic nerve traction force can be so large to even retract the eyeball within its orbit [47]. If such a traction force were to increase in high myopia, then the contribution on collagen remodeling might become more important than that of IOP or CSFP, and collagen fibers may try to orient along the direction of higher stress. In adduction (left eye movement for a right eye), the dura transmits higher stress in the temporal side of the peripapillary sclera, which could plausibly result in a radial alignment of the collagen fibers in that area. Interestingly, in this study we found disrupted collagen fiber orientations in nasal and temporal regions. However, in high myopia several morphological changes, such as the presence of a tilted disc or peripapillary atrophy (delta and gamma zones [48]), may also affect stress distributions within the peripapillary sclera, and other remodeling scenarios may be plausible. Stress levels can also be high in the nasal quadrant of the sclera in abduction [46]. To better understand this phenomenon, we are currently building growth and remodeling computational models to help us tease out the most relevant forces responsible for a change in the collagen fiber orientation.

Several studies have linked a significant increase in the prevalence of glaucoma with high myopia [49-51]. Several authors have reported that highly myopic patients have larger optic discs [5,52,53]. Jonas et al. [52] described them as “secondary acquired macrodisks,” which are accompanied by larger peripapillary atrophic regions. Saw et al. [5] added to the list of abnormalities a tilt to the optic disc, as well as a thinner LC. Bellezza et al. [54] concluded that a larger optic disc is more susceptible to IOP-related damage, which could link to the pathological changes to the scleral architecture presented here. Specifically, in specimen HM2 the scleral canal was noticeably enlarged, with the width of the aligned collagen ring spanning a larger radius than in the control specimens. This could be a direct result of elongation of the eye. Based on the polar vector plot map for HM1, the optic nerve canal appears to be stretched in the ST-IN direction, in which there also a smaller amount of preferentially aligned collagen. This is reminiscent of the findings of Pijanka et al. [12] for glaucomatous specimens, which showed a significantly lower degree of peripapillary collagen alignment in glaucomatous eyes. Furthermore, the Beijing eye study [49] found that although there was no significant difference in IOP between highly myopic and non-myopic eyes, the former group exhibited a significantly higher onset of glaucoma. This could further suggest that a greater risk of developing glaucomatous damage might be linked with structural changes occurring with high myopia, such as those in the peripapillary sclera noted in this study.

Several experimental limitations and factors must be taken into account when drawing conclusions from the present study. First, the number of highly myopic specimens used in the study was small due to the universally limited availability of suitable posterior scleral tissue from donors of known myopic status. Although the structure of all three myopic eyes deviated noticeably from the non-myopic eyes, whose structural features were, in contrast, highly reproducible between specimens (Appendix 3 and Appendix 4), caution should be used when applying the results of the current preliminary work to human high myopia in general without validation in a larger sample population. Second, the axial length of the specimens was not determined. This was compensated by calculating the distance from the edge of the optic nerve canal to the insertion of the inferior oblique muscle for each posterior shell, as a measure of the scleral tissue elongation. Notably, the results were highly consistent between the controls (Table 1), with a marked increase for myopic specimens HM2 and HM3. This calculation could not be performed accurately for HM1 because the widespread nature of the structural deformations present in this specimen precluded the use of the inferior oblique muscle insertion as a reliable landmark. However, the specimen was confirmed to be highly myopic in the clinic, with >6D of refractive error. Nonetheless, further studies are required to correlate axial length with scleral microstructural changes to shed further light on the role of collagen fiber remodeling in myopia progression. Also related to this point, it is unknown if any of the donors from the current study had myopia since early childhood (early onset myopia) or developed myopia later in

life, or in the former case, how the original disease associated with high myopia. How these factors might relate to the microstructural alterations described in the present study warrants further investigation. Third, information about the sex and ethnicity of the donors was not available. Although the potential effect (if any) of sex on the scleral microstructure is not known, there is some documented evidence that collagen fiber arrangement [55] and structural stiffness [56] of the posterior sclera may vary between ethnic groups. Fourth, there are inherent limitations to the WAXS method itself. As mentioned, WAXS yields thickness-averaged results and cannot provide clarity on structural composition throughout the tissue depth. Pijanka et al. [30] showed that the circumferentially aligned collagen fibers do not persist through the entire tissue depth, only in the outer two-thirds of the stroma. Thus, whether the observed changes in the myopic specimens are present through the entire depth of the scleral tissue remains unknown. Flattening of the scleral coat may have released some of the residual stress that is present in the intact tissue, potentially causing changes in the typical collagen fibril orientation. It has been shown, however, that this effect is more profound at a macro- (organ) level and less prominent at the collagen microstructure level [57]. Moreover, the relaxing incisions used to flatten the tissue did not penetrate the peripapillary tissue where the quantitative analysis in this paper was concentrated. In addition, the original fixation of the eye tunic in its natural curvature should have further limited the extent of any fibrillar reorganization upon subsequent dissection. Nevertheless, considering the limited number of specimens available to the study, it was decided not to include the mid-posterior tissue in the quantitative analysis, as minor changes in fiber alignment near the cuts cannot be ruled out.

In conclusion, using WAXS we mapped the bulk posterior scleral collagen structure of three human eyes with high myopia. In comparison to non-myopic eyes, all three highly myopic specimens showed disruptions in the characteristic circumferential collagen fibril organization in the peripapillary sclera, as well as changes in the normally well conserved regional pattern of anisotropic proportion. The results support the idea that pathological structural remodeling takes place with high myopia that accompanies axial lengthening and mechanical alteration of the scleral tissue. Further research is required to ascertain whether these structural changes are a direct result of remodeling of the posterior sclera during axial lengthening or whether they could be a mechanical adaption to tissue stresses induced by fluid pressure or eye movements that may be exacerbated in enlarged eyes. Structural changes in the peripapillary region may link to the increased susceptibility of myopic eyes to glaucoma development. The present data will enhance future modeling studies of ocular biomechanical changes in myopia and glaucoma.

APPENDIX 1.

Idealized mathematical polar vector distribution for perfect circumferential alignment, used to compare control and myopic collagen orientation in the largely circumferential peripapillary region. Numerical values from 0 to 180 degrees denote the main orientation angle. To access the data, click or select the words “Appendix 1.”

APPENDIX 2.

Comparison of mean collagen anisotropic proportion by quadrant for non-myopic control group specimens. Minimum and maximum values for each specimen (denoted by – and + symbols) are consistently observed in the SN and IN quadrants, respectively. To access the data, click or select the words “Appendix 2.”

APPENDIX 3.

WAXS polar plot vector maps of three non-myopic (A-F) posterior scleras. (A) Full map of non-myopic specimen N1; (B) 30 × 30 vector plot zoom of N1; (C) Full map of non-myopic specimen N2; (D) 30 × 30 vector plot zoom of N2; (E) Full map of non-myopic specimen N3; (F) 30 × 30 vector plot zoom of N3. The zoomed regions are denoted by a red square on the full maps. Peripapillary scleral region is shown bounded by black lines. Discontinuations of the circumferential collagen orientation in the SN quadrant are indicated by arrows. S, N, I and T denote superior, nasal, inferior and temporal directions, respectively. To access the data, click or select the words “Appendix 3.”

APPENDIX 4.

WAXS polar plot vector maps of three non-myopic (A-F) posterior scleras. (A) Full map of non-myopic specimen N5; (B) 30 × 30 vector plot zoom of N5; (C) Full map of non-myopic specimen N6; (D) 30 × 30 vector plot zoom of N6; (E) Full map of non-myopic specimen N7; (F) 30 × 30 vector plot zoom of N7. The zoomed regions are denoted by a red square on the full maps. Peripapillary scleral region is shown bounded by black lines. Discontinuations of the circumferential collagen orientation in the SN quadrant are indicated by arrows. S, N, I and T denote superior, nasal, inferior and temporal directions, respectively. To access the data, click or select the words “Appendix 4.”

ACKNOWLEDGMENTS

The authors thank Ahmed Abass and Martin Spang for technical contributions and Diamond Light Source for access to beamlines I02 and I03. This work was supported by funding from the EPSRC, STFC and NIH (NEI R01EY021500 - subaward 2003284605).

REFERENCES

1. Holden BA, Fricke TR, Wilson DA, Jong M, Naidoo KS, Sankaridurg P, Wong TY, Naduvilath TJ, Resnikoff S. Global prevalence of myopia and high myopia and temporal trends from 2000 through 2050. Ophthalmology 2016; 123:1036-42. [PMID: 26875007].
2. Wu LJ, You QS, Duan JL, Luo YX, Liu LJ, Li X, Gao Q, Zhu HP, He Y, Xu L, Jonas JB, Wang W, Guo XH. Prevalence and associated factors of myopia in high-school students in Beijing. PLoS One 2015; 10:e0120764-[PMID: 25803875].
3. Lee MW, Kim JM, Shin YI, Jo YJ, Kim JY. Longitudinal Changes in Peripapillary Retinal Nerve Fiber Layer Thickness in High Myopia: A Prospective, Observational Study. Ophthalmology 2018; [Epub ahead of print][PMID: 30195452].
4. Verkicharla PK, Ohno-Matsui K, Saw SM. Current and predicted demographics of high myopia and an update of its associated pathological changes. Ophthalmic Physiol Opt 2015; 35:465-75. [PMID: 26303444].
5. Saw SM, Gazzard G, Shih□Yen EC, Chua WH. Myopia and associated pathological complications. Ophthalmic Physiol Opt 2005; 25:381-91. [PMID: 16101943].
6. Holden B, Sankaridurg P, Smith E, Aller T, Jong M, He M. Myopia, an underrated global challenge to vision: where the current data takes us on myopia control. Eye (Lond) 2014; 28:142-6. [PMID: 24357836].
7. McBrien NA, Gentle A. Role of the sclera in the development and pathological complications of myopia. Prog Retin Eye Res 2003; 22:307-38. [PMID: 12852489].
8. Watson PG, Young RD. Scleral structure, organisation and disease. A review. Exp Eye Res 2004; 78:609-23. [PMID: 15106941].
9. Komai Y, Ushiki T. The three-dimensional organization of collagen fibrils in the human cornea and sclera. Invest Ophthalmol Vis Sci 1991; 32:2244-58. [PMID: 2071337].
10. Shoulders MD, Raines RT. Collagen structure and stability. Annu Rev Biochem. Vol 78. Palo Alto: Annual Reviews; 2009. p. 929–58.
11. Hogan M. JA A, JE W. Histology of the human eye: Philadelphia: WB Saunders; 1971.
12. Pijanka JK, Coudrillier B, Ziegler K, Sorensen T, Meek KM, Nguyen TD, Quigley HA, Boote C. Quantitative mapping of collagen fiber orientation in non-glaucoma and glaucoma posterior human sclerae. Invest Ophthalmol Vis Sci 2012; 53:5258-70. [PMID: 22786908].
13. Pijanka JK, Abass A, Sorensen T, Elsheikh A, Boote C. A wide-angle X-ray fibre diffraction method for quantifying collagen orientation across large tissue areas: application to the human eyeball coat. J Appl Cryst 2013; 46:1481-9. .
14. Girard MJA, Downs JC, Bottlang M, Burgoyne CF, Suh JKF. Peripapillary and posterior scleral mechanics-Part II: Experimental and inverse finite element characterization. J Biomech Eng-T Asme 2009; 131:1-10. [PMID: 19388782].
15. Strouthidis NG, Girard MJA. Altering the way the optic nerve head responds to intraocular pressure—a potential approach to glaucoma therapy. Curr Opin Pharmacol 2013; 13:83-9. [PMID: 22999652].
16. Sigal IA, Yang H, Roberts MD, Burgoyne CF, Downs JC. IOP-induced lamina cribrosa displacement and scleral canal expansion: an analysis of factor interactions using parameterized eye-specific models. Invest Ophthalmol Vis Sci 2011; 52:1896-907. [PMID: 20881292].
17. McBrien NA. Regulation of scleral metabolism in myopia and the role of transforming growth factor-beta. Exp Eye Res 2013; 114:128-40. [PMID: 23399866].
18. Jonas JB, Xu L. Histological changes of high axial myopia. Eye (Lond) 2014; 28:113-7. [PMID: 24113300].
19. Flores-Moreno I, Lugo F, Duker JS, Ruiz-Moreno JM. The relationship between axial length and choroidal thickness in eyes with high myopia. Am J Ophthalmol 2013; 155:314-9. [PMID: 23036569].
20. Harper AR, Summers JA. The dynamic sclera: Extracellular matrix remodeling in normal ocular growth and myopia development. Exp Eye Res 2015; 133:100-11. [PMID: 25819458].
21. McBrien NA, Jobling AI, Gentle A. Biomechanics of the sclera in myopia: extracellular and cellular factors. Optom Vis Sci 2009; 86:E23-30. [PMID: 19104466].
22. Jones BE, Thompson EW, Hodos W, Waldbillig R, Chader GJ. Scleral matrix metalloproteinases, serine proteinase activity and hydrational capacity are increased in myopia induced by retinal image degradation. Exp Eye Res 1996; 63:369-81. [PMID: 8944544].
23. Gentle A, Liu Y, Martin JE, Conti GL, McBrien NA. Collagen gene expression and the altered accumulation of scleral collagen during the development of high myopia. J Biol Chem 2003; 278:16587-94. [PMID: 12606541].
24. McBrien NA, Cornell LM, Gentle A. Structural and ultrastructural changes to the sclera in a mammalian model of high myopia. Invest Ophthalmol Vis Sci 2001; 42:2179-87. [PMID: 11527928].
25. Guggenheim JA, McBrien NA. Form-deprivation myopia induces activation of scleral matrix metalloproteinase-2 in tree shrew. Invest Ophthalmol Vis Sci 1996; 37:1380-95. [PMID: 8641841].
26. McBrien NA, Metlapally R, Jobling AI, Gentle A. Expression of collagen-binding integrin receptors in the mammalian sclera and their regulation during the development of myopia.

Invest Ophthalmol Vis Sci 2006; 47:4674-82. [PMID: 17065473].

27. Boote C, Palko JR, Sorensen T, Mohammadvali A, Elsheikh A, Komaromy AM, Pan XL, Liu J. Changes in posterior scleral collagen microstructure in canine eyes with an ADAMTS10 mutation. Mol Vis 2016; 22:503-17. [PMID: 27212875].

28. Meek KM, Boote C. The use of x-ray scattering techniques to quantify the orientation and distribution of collagen in the corneal stroma. Prog Retin Eye Res 2009; 28:369-92. [PMID: 19577657].

29. Coudrillier B, Boote C, Quigley HA, Nguyen TD. Scleral anisotropy and its effects on the mechanical response of the optic nerve head. Biomech Model Mechanobiol 2013; 12:941-63. [PMID: 23188256].

30. Pijanka JK, Spang MT, Sorensen T, Liu J, Nguyen TD, Quigley HA, Boote C. Depth-dependent changes in collagen organization in the human peripapillary sclera. PLoS One 2015; 10:1-17. [PMID: 25714753].

31. Pijanka JK, Kimball EC, Pease ME, Abass A, Sorensen T, Nguyen TD, Quigley HA, Boote C. Changes in scleral collagen organization in murine chronic experimental glaucoma. Invest Ophthalmol Vis Sci 2014; 55:6554-64. [PMID: 25228540].

32. Winkler M, Jester B, Nien-Shy C, Massei S, Minckler DS, Jester JV, Brown DJ. High resolution three-dimensional reconstruction of the collagenous matrix of the human optic nerve head. Brain Res Bull 2010; 81:339-48. [PMID: 19524027].

33. Coudrillier B, Pijanka J, Jefferys J, Sorensen T, Quigley HA, Boote C, Nguyen TD. Collagen structure and mechanical properties of the human sclera: Analysis for the effects of age. J Biomech Eng-T Asme 2015; 137:1-14. [PMID: 25531905].

34. Summers Rada JA, Shelton S, Norton TT. The sclera and myopia. Exp Eye Res 2006; 82:185-200. [PMID: 16202407].

35. Roberts MD, Grau V, Grimm J, Reynaud J, Bellezza AJ, Burgoyne CF, Downs JC. Remodeling of the connective tissue microarchitecture of the lamina cribrosa in early experimental glaucoma. Invest Ophthalmol Vis Sci 2009; 50:681-90. [PMID: 18806292].

36. Girard MJA, Dahlmann-Noor A, Rayapureddi S, Bechara JA, Bertin BME, Jones H, Albon J, Khaw PT, Ethier CR. Quantitative mapping of scleral fiber orientation in normal rat eyes. Invest Ophthalmol Vis Sci 2011; 52:9684-93. [PMID: 22076988].

37. Jan N-J, Lathrop K, Sigal IA. Collagen architecture of the posterior pole: High-resolution wide field of view visualization and analysis using polarized light microscopyposterior pole collagen architecture. Invest Ophthalmol Vis Sci 2017; 58:735-44. [PMID: 28146238].

38. Jan N-J, Grimm JL, Tran H, Lathrop KL, Wollstein G, Bilonick RA, Ishikawa H, Kagemann L, Schuman JS, Sigal IA. Polarization microscopy for characterizing fiber orientation of ocular tissues. Biomed Opt Express 2015; 6:4705-18. [PMID: 26713188].

39. Grytz R, Meschke G, Jonas JB. The collagen fibril architecture in the lamina cribrosa and peripapillary sclera predicted by a computational remodeling approach. Biomech Model Mechanobiol 2011; 10:371-82. [PMID: 20628781].

40. Girard MJA, Downs JC, Burgoyne CF, Suh JKF. Peripapillary and posterior scleral mechanics-Part I: Development of an anisotropic hyperelastic constitutive model. J Biomech Eng-T Asme 2009; 131:1-9. [PMID: 19388781].

41. Coudrillier B, Pijanka JK, Jefferys JL, Goel A, Quigley HA, Boote C, Nguyen TD. Glaucoma-related changes in the mechanical properties and collagen micro-architecture of the human sclera. PLoS One 2015; 10:21-[PMID: 26161963].

42. Jones H, Girard M, White N, Fautsch MP, Morgan J, Ethier C, Albon J. Quantitative analysis of three-dimensional fibrillar collagen microstructure within the normal, aged and glaucomatous human optic nerve head. J R Soc Interface 2015; 12:1-12. [PMID: 25808336].

43. Grytz R, Fazio MA, Libertiaux V, Bruno L, Gardiner S, Girkin CA, Downs JC. Age- and race-related differences in human scleral material properties. Invest Ophthalmol Vis Sci 2014; 55:8163-72. [PMID: 25389203].

44. Campbell IC, Coudrillier B, Ross Ethier C. Biomechanics of the posterior eye: a critical role in health and disease. J Biomech Eng 2014; 136:1-19. [PMID: 24356942].

45. Jonas JB, Dai Y, Panda-Jonas S. Peripapillary Suprachoroidal Cavitation, Parapapillary Gamma Zone and Optic Disc Rotation Due to the Biomechanics of the Optic Nerve Dura Mater. Invest Ophthalmol Vis Sci 2016; 57:4373-[PMID: 27557435].

46. Wang X, Fisher LK, Milea D, Jonas JB, Girard MJA. Predictions of Optic Nerve Traction Forces and Peripapillary Tissue Stresses Following Horizontal Eye Movements. Invest Ophthalmol Vis Sci 2017; 58:2044-53. [PMID: 28384725].

47. Demer JL. Optic nerve sheath as a novel mechanical load on the globe in ocular duction. Invest Ophthalmol Vis Sci 2016; 57:1826-38. [PMID: 27082297].

48. Jonas JB, Fang Y, Weber P, Ohno-Matsui K. Parapapillary Gamma and Delta Zones in High Myopia. Retina 2018; 38:931-8. [PMID: 28426626].

49. Xu L, Wang Y, Wang S, Wang Y, Jonas JB. High myopia and glaucoma susceptibility: The Beijing eye study. Ophthalmology 2007; 114:216-20. [PMID: 17123613].

50. Leske MC, Connell A, Schachat AP, Hyman L. The Barbados Eye Study: prevalence of open angle glaucoma. Arch Ophthalmol 1994; 112:821-9. [PMID: 8002842].

51. Mitchell P, Hourihan F, Sandbach J, Jin Wang J. The relationship between glaucoma and myopia: The Blue Mountains eye study. Ophthalmology 1999; 106:2010-5. [PMID: 10519600].

52. Jonas JB, Gusek GC, Naumann GO. Optic disk morphometry in high myopia. Graefes Arch Clin Exp Ophthalmol 1988; 226:587-90. [PMID: 3209086].

53. Kimura Y, Akagi T, Hangai M, Takayama K, Hasegawa T, Suda K, Yoshikawa M, Yamada H, Nakanishi H, Unoki N. Lamina cribrosa defects and optic disc morphology in

primary open angle glaucoma with high myopia. PLoS One 2014; 9:1-18. [PMID: 25531656].

54. Bellezza AJ, Hart RT, Burgoyne CF. The optic nerve head as a biomechanical structure: Initial finite element modeling. Invest Ophthalmol Vis Sci 2000; 41:2991-3000. [PMID: 10967056].

55. Yan D, McPheeters S, Johnson G, Utzinger U, Vande Geest JP. Microstructural differences in the human posterior sclera as a function of age and race. Invest Ophthalmol Vis Sci 2011; 52:821-9. [PMID: 21051726].

56. Fazio MA, Grytz R, Morris JS, Bruno L, Girkin CA, Downs JC. Human scleral structural stiffness increases more rapidly with age in donors of African descent compared to donors of European descent. Invest Ophthalmol Vis Sci 2014; 55:7189-98. [PMID: 25237162].

57. Lanir Y. Mechanisms of residual stress in soft tissues. J Biomech Eng 2009; 131:1-5. [PMID: 19275448].

Articles are provided courtesy of Emory University and the Zhongshan Ophthalmic Center, Sun Yat-sen University, P.R. China. The print version of this article was created on 30 December 2018. This reflects all typographical corrections and errata to the article through that date. Details of any changes may be found in the online version of the article.